

Radiative Thermalisation at the Nanoscale

Author: Sebastià Feliu Juárez.

Facultat de Física, Universitat de Barcelona, Diagonal 645, 08028 Barcelona, Spain.

Advisor: Ivan Latella

Abstract: Radiative heat transfer at the nanometre scale can be several orders of magnitude higher than predicted by the Stefan-Boltzmann law. When the distance between objects is small compared to the thermal wavelength, evanescent waves contribute significantly to the heat transfer, so that the blackbody limit can be exceeded. This is especially important when considering the thermalisation between two objects that are in close proximity and exchange heat by thermal radiation. In this project, radiative thermalisation is investigated theoretically and numerically in the particular case of two bodies and a thermal bath. The stationary temperature of one of the bodies is studied as a function of the separation distance between the objects and it is shown that the thermalisation induces a saturation of the heat flow.

I. Introduction

The Stefan-Boltzmann law states that the power radiated per unit area from a blackbody in thermal equilibrium is proportional to the fourth power of its temperature [1], which constitutes an important tool to describe the radiative heat transfer between objects out of contact. This law is valid when the bodies exchanging energy are separated by large distances. When the separations are below the characteristic wavelength of the thermal radiation, a different theoretical framework is needed to describe the heat exchange [2].

The mechanism of radiative heat transfer originates from the random thermal movement of charges within objects, such as electrons in metals or ions in polar materials, which generate fluctuating electric currents. According to Maxwell's equations, these currents create fluctuating electromagnetic (EM) fields around the material. It is these fields that mediate the energy transfer through the vacuum between bodies, especially at sufficiently small distances where the energy flux can be accurately predicted by means of the fluctuational electrodynamics approach [2–4].

The radiative heat exchange is classified into far-field and near-field regimes depending on the separation distance d between the objects relative to the thermal wavelength λ_T . In the far-field regime, for which $d \gg \lambda_T$, the Stefan-Boltzmann law applies and the radiative transfer is realised via propagating waves, so the energy exchange does not depend on the distance. In contrast, for $d < \lambda_T$, in the near-field regime, there is a significant contribution from evanescent waves, which arise from frustrated total internal reflection and decay exponentially with the distance from the interface, increasing heat transfer beyond the blackbody limit [2–4].

In this final degree project, we study the radiative heat transfer between two bodies made of the same material interacting with a thermal bath; one of the bodies is considered semi-infinite (a half-space) and the other body is a suspended membrane which is assumed optically opaque (in practice, it is semi-infinite as well). By

letting free the temperature of the membrane and keeping the other temperatures fixed, we investigate the thermalisation process that takes place when the separation distance between the bodies is reduced close to contact. Here we follow the approach proposed in [5] and, as discussed in this reference, we show that the heat flux between the bodies saturates at short distances due to the process of thermalisation.

This work has the following structure: In Sec. II the system under study is introduced. In Sec. III the theoretical framework of radiative heat transfer in the near-field regime is described, including specific formulas adapted to the proposed setup. In Sec. IV, we numerically investigate the thermalisation process, in particular the transmission coefficients, the equilibrium temperature of the membrane and the energy flux. Finally, in Sec. V final remarks are presented.

II. The system: stationary temperatures and thermalisation

The system under consideration, depicted in Fig. 1, consists of a substrate (body 1) and an opaque membrane (body 2) interacting with a thermal bath of radiation which plays the role of a third body. The membrane is placed at a separation distance d from the substrate whereas the thermal bath at fixed temperature T_3 acts on the membrane from the other side. The substrate is maintained at a constant temperature T_1 , while the temperature of the membrane T_2 is not fixed. Here we consider that both substrate and membrane are made of the same material, either silicon carbide (SiC) or gold (Au).

As illustrated in Fig. 1, $\Phi_1(T_2)$ represents the thermal radiation energy flux in the vacuum region between body 1 and body 2, and $\Phi_2(T_2)$ denotes the flux to the right of body 2. While T_1 and T_3 are held fixed, these fluxes depend on the temperature of the intermediate body which is free to reach the steady state value $T_2 = T_2^{st}$. This stationary temperature is obtained by requiring that the

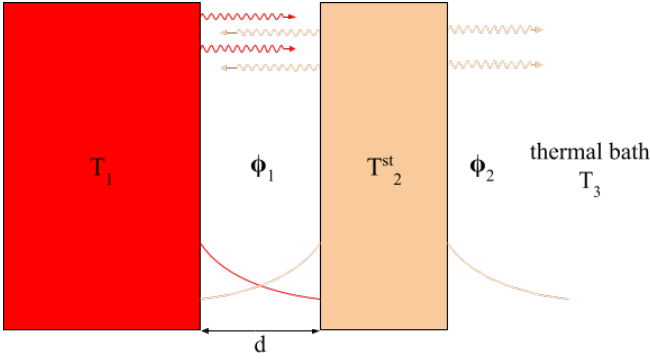


FIG. 1: System setup showing the two semi-infinite bodies the membrane and the substrate, and the thermal bath. The temperatures of the bodies and the fluxes are shown. The figure also highlights the two mechanisms for heat exchange, the propagative and evanescent modes.

net energy flux on the membrane vanishes, hence

$$\Phi_1(T_2^{st}) - \Phi_2(T_2^{st}) = 0. \quad (1)$$

This equilibrium condition implies that the fluxes on the left and on the right of the membrane take the same value, namely, the energy flux

$$\Phi \equiv \Phi_1(T_2^{st}) = \Phi_2(T_2^{st}). \quad (2)$$

Furthermore, radiative heat fluxes in the near field strongly increase as the separation distance d is decreased (explicit expressions are given below in Sec. III). As this separation is reduced at the same time that the membrane is allowed to reach a thermal steady state, its temperature T_2^{st} increases due to near-field heat exchange with body 1 maintained at temperature $T_1 > T_2^{st}$. In this way, the temperature difference $\Delta T \equiv T_1 - T_2^{st}$ decreases to zero close to contact due to the near-field interaction between the bodies, resulting in the thermalisation of the membrane. In the following, we first describe the radiative heat fluxes in the system and in Sec. IV we apply these concepts to characterise the thermalisation process.

III. Near-field radiative heat transfer

The stochastic motion of charges produced by thermal excitations inside the materials leads to the emission of EM fields. The energy per unit surface and unit time at a point \mathbf{R} and time t in each vacuum region γ is given by the Poynting vector $\mathbf{S}^\gamma(\mathbf{R}, t) = \epsilon_0 c^2 \mathbf{E}^\gamma(\mathbf{R}, t) \times \mathbf{B}^\gamma(\mathbf{R}, t)$, where ϵ_0 is the vacuum permittivity, c is the speed of light in vacuum, and $\mathbf{E}^\gamma(\mathbf{R}, t)$ and $\mathbf{B}^\gamma(\mathbf{R}, t)$ are the electric and magnetic fields radiated by the bodies, respectively. Here, $\gamma = 1$ labels the region between body 1 and body 2, while $\gamma = 2$ indicates the region on the right of body 2. Although these fields are zero on average, their correlations do not vanish and are related to the temperature by means of the fluctuation-dissipation theorem [2], allowing for energy transfer mediated by the emitted radiation.

Considering the surfaces of the bodies as infinite and lying on the x - y plane, the thermal-radiation energy flux is given by the averaged component of the Poynting vector perpendicular to the surfaces,

$$\Phi_\gamma \equiv \langle S_z^\gamma(R, t) \rangle = \epsilon_0 c^2 \sum_{j,k} \epsilon_{zjk} \langle E_j^\gamma(R, t) B_k^\gamma(R, t) \rangle, \quad (3)$$

where $\langle \dots \rangle$ means symmetrized statistical average and ϵ_{ijk} is the Levi-Civita tensor with $i, j, k = x, y, z$. By expanding the EM field into plane-wave components, which are defined by frequency ω , parallel wave vector k , and polarisation states $p = \text{TE}, \text{TM}$, the energy flux within each vacuum region γ in many-body systems can be written as [6]

$$\Phi_\gamma = \int_0^\infty \frac{d\omega}{2\pi} \int_0^\infty \frac{dk}{2\pi} k \sum_p \sum_{j=1}^2 \hbar \omega n_{j,j+1} \mathcal{T}_j^\gamma(k, \omega, p). \quad (4)$$

Here we have introduced $n_{ij} \equiv n_i - n_j$, where $n_j = 1/(e^{\hbar\omega/k_B T_j} - 1)$ is the Bose-Einstein distribution function of body j , k_B being the Boltzmann constant and \hbar the reduced Planck constant. For the proposed system, the non-zero energy transmission coefficients can be obtained from fluctuational electrodynamics and are given by [6]

$$\begin{aligned} \mathcal{T}_1^1(k, \omega, p) &= \Pi^{\text{pw}} \frac{(1 - |r_1^p|^2)(1 - |r_2^p|^2)}{|1 - r_1^p r_2^p e^{i2k_z d}|^2} \\ &\quad + \Pi^{\text{ew}} \frac{4\text{Im}(r_1^p)\text{Im}(r_2^p) e^{-2\text{Im}(k_z)d}}{|1 - r_1^p r_2^p e^{-2\text{Im}(k_z)d}|^2}, \\ \mathcal{T}_2^2(k, \omega, p) &= \Pi^{\text{pw}} (1 - |r_2^p|^2), \end{aligned} \quad (5)$$

where $\Pi^{\text{pw}} = \theta(\omega - ck)$ and $\Pi^{\text{ew}} = \theta(ck - \omega)$ are the projectors for propagating and evanescent waves, respectively, $\theta(x)$ being the Heaviside step function. The Fresnel reflection coefficients r_j^p for the vacuum-medium interfaces are given by

$$r_j^{\text{TE}} = \frac{k_z - k_{zj}}{k_z + k_{zj}}, \quad r_j^{\text{TM}} = \frac{\epsilon_j k_z - k_{zj}}{\epsilon_j k_z + k_{zj}}, \quad (6)$$

where $k_{zj} = \sqrt{\omega^2 \epsilon_j(\omega)/c^2 - k^2}$ is the perpendicular component of the wavevector in medium j . According to the above expressions, the heat transfer between the bodies can be computed by describing the permittivity of the involved materials.

IV. Numerical application

The radiative energy fluxes in the near field, in general, are obtained numerically. Before explaining the scheme of our numerical calculation, we first describe the models we use for the optical properties of the materials and the transmission coefficients that account for these properties.

A. Optical properties

The materials considered for both bodies are either SiC, a polar material, or Au, a metal. For SiC the permittivity is given by the Drude-Lorentz model [8]

$$\epsilon(\omega) = \epsilon_\infty \frac{\omega_L^2 - \omega^2 - i\Gamma\omega}{\omega_T^2 - \omega^2 - i\Gamma\omega}, \quad (7)$$

where $\epsilon_\infty = 6.7$ is the infinite-frequency dielectric constant, $\omega_L = 1.83 \times 10^{14}$ rad/s is the longitudinal optical frequency, $\omega_T = 1.49 \times 10^{14}$ rad/s is the transverse optical frequency, and $\Gamma = 8.97 \times 10^{11}$ rad/s is the damping rate. For Au the permittivity is described by the Drude model [9]

$$\epsilon(\omega) = 1 - \frac{\omega_P^2}{\omega^2 + i\nu\omega}, \quad (8)$$

where $\omega_P = 1.37 \times 10^{16}$ rad/s represents the plasma frequency and $\nu = 5.32 \times 10^{13}$ denotes the electron collision frequency.

B. Energy transmission coefficients

It is important to highlight some of the features of the energy transmission coefficients as they exhibit underlying material properties. We show these coefficients in Figs. 2 and 3, where the light line $\omega = ck$ is plotted in yellow to differentiate propagating, on the left of this line, from evanescent modes on the right. In Fig. 2, we set $d = 50$ nm (near-field regime) in region $\gamma = 1$ and represent the transmission coefficient for TM polarisation for both materials to illustrate the material resonances. For the polar material (SiC), a resonance can be observed at the top panel of Fig. 2 which is called surface-phonon polariton and emerges as a coupling of an electromagnetic wave with an optical phonon. The frequency of these phonon polaritons is in the infrared region and can be thermally excited because, for the temperatures considered here, the Bose-Einstein distribution is non-zero in this region. Therefore the main contribution to heat transfer in the near-field regime arises from this resonance.

In the case of the metal (Au), the resonance that can be seen in the bottom panel of Fig. 2 is called surface plasmon polariton, which is a surface EM wave that travels along the interface between the metal and the vacuum, coupled with the collective oscillations of free electrons in the metal. Unlike for polar materials, these resonances typically occur in the visible or ultraviolet, so they are out of the Planck Window at the close-to-room temperatures considered here (i.e. the interval where the Bose-Einstein distribution is non-zero) and do not contribute to heat transfer.

In the case of the \mathcal{T}_2^2 coefficients, instead of a maximum contribution line, a small contribution interval is observed in the reststrahlen band. This band corresponds

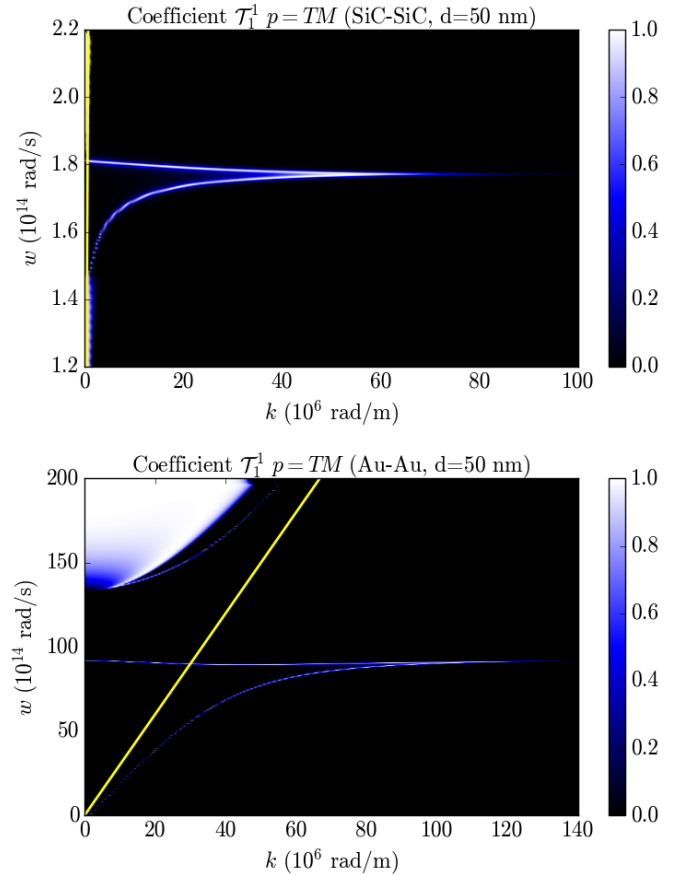


FIG. 2: Energy transmission coefficients \mathcal{T}_1^1 for TM polarisation for both materials: the top of the panel corresponds to SiC and the bottom to Au. Here the separation between the bodies is $d = 50$ nm (near-field regime). The yellow solid line shows the light line $\omega = ck$.

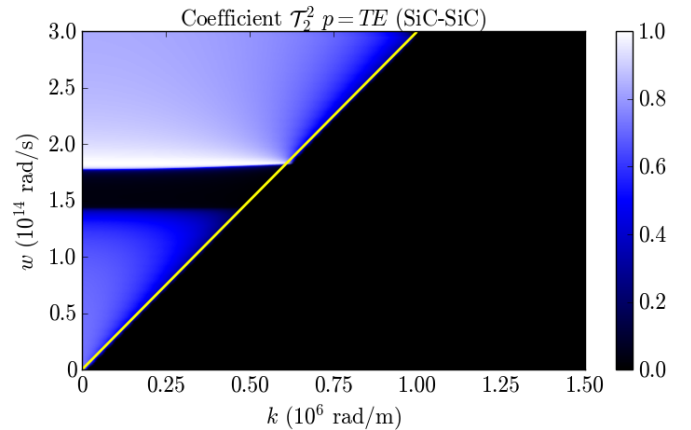


FIG. 3: Energy transmission coefficients \mathcal{T}_2^2 for TE polarisation for the polar material at a large separation (far-field regime). The yellow solid line shows the light line $\omega = ck$.

to the frequency range in which the above-mentioned resonance occurs (i.e. when $\text{Re}[\epsilon(\omega)] = -1$). This band appears precisely because, in the absence of a second in-

interface on the right side of the membrane, the evanescent waves are quickly extinguished when they leave the membrane interface and do not contribute to heat propagation. Therefore, in the $\gamma = 2$ region, only the propagating modes contribute. As a representative plot, the coefficient \mathcal{T}_2^2 for $p = \text{TE}$ is shown in Fig. 3.

C. Steady state temperature and energy flux saturation

A Fortran program was developed to compute the energy transmission coefficients defined in equation (5) for given values of ω , k , p , and separation distance d . This was used by another program to calculate the flux in each region by bidimensional numerical integration over ω and k , using the trapezoidal method. To facilitate integration over the infinite interval [see equation (4)], a change of variables was implemented that permits integration in the interval $[0, 1]$. Furthermore, since the temperature of the membrane T_2 is not predetermined, it is allowed to adjust to a steady-state value T_2^{st} such that the net energy flux on the membrane is zero. To determine this variable temperature at a given value of the separation d , a third Fortran program was written using the Newton-Raphson method to solve the equilibrium condition in equation (1). All numerical calculations were performed at constant temperatures $T_1 = 400 \text{ K}$ for body 1 and $T_3 = 300 \text{ K}$ for the thermal bath.

In Fig. 4 we show the stationary temperature T_2^{st} and the heat flux Φ in the cavity, given by equation (2), for the case in which the two bodies are made of SiC. On the one hand, at small separations, the TM polarisation dominates the heat flux because of the contribution of the surface phonon polariton and the flux behaves as [5]

$$\Phi = \frac{1}{d^2} \int_0^\infty \frac{d\omega}{2\pi} \hbar \omega n_{1,2} \frac{\text{Im}^2[r(\omega)] \text{Im}[\text{Li}_2(r^2(\omega))]}{2\pi \text{Im}(r^2)}, \quad (9)$$

where $r(\omega)$ is the Fresnel coefficient and $\text{Li}_2(x)$ is the dilogarithm function. On the other hand, as shown in the inset of this figure, at small distances the temperature difference $\Delta T = T_1 - T_2^{st}$ decreases to zero according to d^2 , evidencing the thermalisation of the membrane at the temperature of body 1. Hence, the difference of distributions $n_{1,2} = n_1 - n_2$ in equation (9) can be linearised for small ΔT in such a way that $n_{1,2} \approx (\partial n_1 / \partial T_1) \Delta T \sim d^2$, which cancel out the $1/d^2$ behaviour of Φ . Thus, as a consequence of the thermalisation of the membrane, the heat flux saturates in the limit of small d . Interestingly, despite working at distances where purely local effects are involved, a saturation of the energy flux due to thermalisation and the presence of the thermal bath can be observed. At large distances (far-field regime), the flux decays to a constant value different from zero and the equilibrium temperature reaches a value higher than the temperature of the thermal bath. This is because the system is semi-infinite.

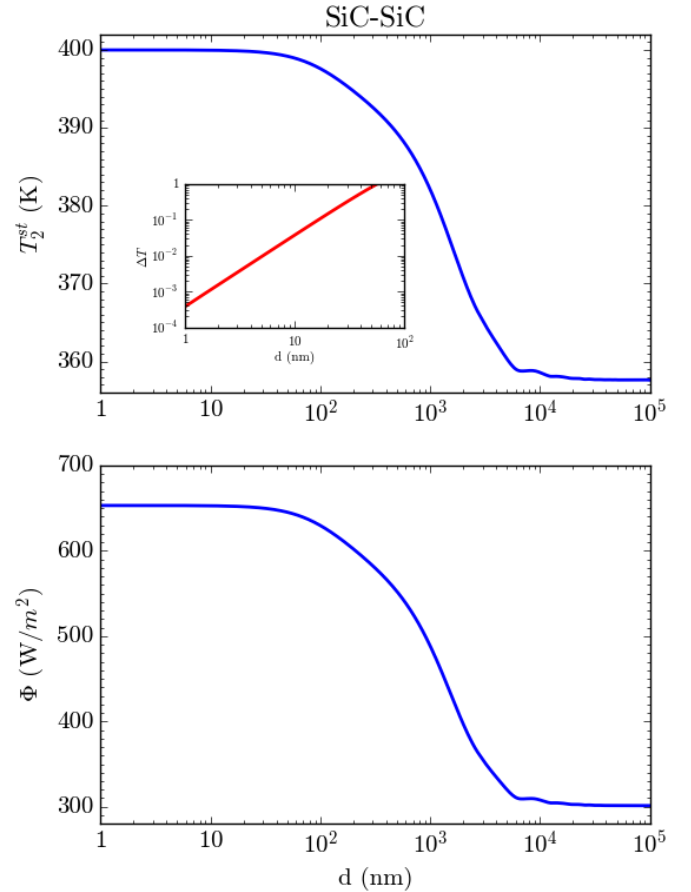


FIG. 4: Steady state temperature of the membrane T_2^{st} and radiative heat flux as a function of the separation d . The inset plots $\Delta T = T_1 - T_2^{st}$ for small values of d . Both bodies are made of SiC.

In Fig. 5 we show the stationary temperature and the heat flux in the cavity for the case of Au. In the inset of this figure, it can be seen that ΔT does not follow the dependence d^2 because the surface plasmon polaritons are not excited at the considered temperatures of the problem. Therefore, the flux between Au-Au is orders of magnitude smaller than that between SiC-SiC. However, for distances smaller than one nanometre ($d \approx 10^{-3} \text{ nm}$), this behaviour would be observed due to the resonance of those surface plasmon polaritons. Then the typical behaviour of $\Delta T \propto d^2$ or flux as $\Phi \propto 1/d^2$ seen so far would manifest on subnanometric scales, and furthermore, the divergence at $d \rightarrow 0$ would be overcome by the non-local effects such as electron tunnelling.

At distances $d > 1 \text{ nm}$, the dominant polarisation is the TE for Au and the effects are purely local [10]. Also in this case the flux saturates at small separations due to thermalisation in the presence of the thermal bath. At larger distances, the flux and temperature decay to a constant value due to the symmetry of the system. Oscillations are observed due to the nonlinear nature of the energy transmission coefficients.

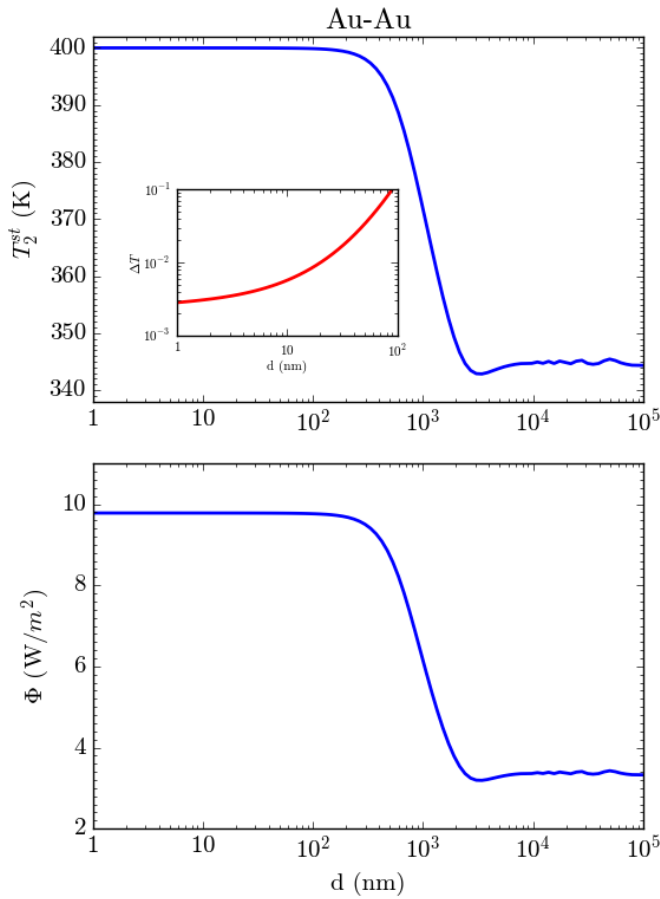


FIG. 5: Steady state temperature of the membrane T_2^{st} and radiative heat flux as a function of the separation d . The inset plots $\Delta T = T_1 - T_2^{st}$ for small values of d . Both bodies are made of Au.

V. Conclusion

To summarise, we have studied the radiative heat transfer between objects at the nanoscale and observed that it increases significantly when the distance is less than the thermal wavelength [2], beyond the blackbody limit given by the Stefan-Boltzmann law. It has been ob-

served that the transmission coefficients greatly depend on the polarisation states (TE and TM modes) and the properties of each material. In particular, for polar materials such as SiC, the TM polarisation dominates due to surface phonon polaritons, which contribute significantly to the heat transfer in the proposed scheme. In contrast, in metals such as Au, surface plasmon polaritons are not excited and the heat flux is typically lower than in polar materials.

It also has been shown that the heat flux saturates due to the thermalisation mechanism caused by the presence of the thermal bath. Typically, the flux scales according to $1/d^2$ and does not diverge close to contact due to predominantly non-local effects on subnanometric scales. However, saturation has been observed at larger scales where these effects are negligible and only local effects are present.

One potential application of radiative heat transfer at nanometre scales is thermophotovoltaic (TPV) technology [11]. Unlike traditional photovoltaic systems that convert sunlight into electricity, this technology converts heat radiation into electricity using photovoltaic (PV) cells. In these systems, the distance between the heat source and the PV cell is reduced to the nanometric scale. Depending on the manufacturing material, photon tunnelling can be achieved in the IR (e.g. SiC) or at higher frequencies, which would imply higher source temperatures. Reducing the distance between the cells and the heat source significantly increases the energy efficiency of TPV systems. The main technical challenge of this technology is to keep the separation distance constant at the nanometre scale and to scale it up to larger devices [12].

Acknowledgments

First and foremost, I would like to thank Professor Ivan for all the insights and discussions that were essential to this project. I would also like to thank my colleagues for their support and encouragement throughout this work. Special thanks to my family for their constant support and motivation.

-
- [1] M. Planck, *The Theory of Heat Radiation* (P. Blakiston's Son & Co., 1914).
 - [2] D. Polder and M. van Hove, *Phys. Rev. B* **4**, 3303 (1971).
 - [3] J. B. Pendry, *J. Phys.: Condens. Matter* **11**, 6621 (1999).
 - [4] K. Joulain, J.-P. Mulet, F. Marquier, R. Carminati, and J.-J. Greffet, *Surf. Sci. Rep.* **57**, 59-112 (2005).
 - [5] I. Latella, R. Messina, S.-A. Biehs, J. M. Rubi and P. Ben-Abdallah. *Sci. Rep.* **10**, 8938 (2020).
 - [6] I. Latella, P. Ben-Abdallah, S.-A. Biehs, M. Antezza and R. Messina. *Phys. Rev. B* **95**, 205404 (2017).
 - [7] B. Juliá and M. Ibañes, *Física Computacional* (2021).
 - [8] E. Palik (Editor), *Handbook of Optical Constants of Solids* (Academic Press, New York, 1998).
 - [9] M. A. Ordal, Robert J. Bell, R. W. Alexander, L. L. Long, and M. R. Querry, *Appl. Opt.* **24**, 4493 (1985).
 - [10] P.-O. Chapuis, S. Volz, C. Henkel, K. Joulain and J.-J. Greffet, *Phys. Rev. B* **77**, 035431 (2008).
 - [11] S. Basu, Z. M. Zhang and C. J. Fu, *Int. J. Energy Res.* **33**, 1203-1232 (2009).
 - [12] B. Song, A. Fiorino, E. Meyhofer and P. Reddy, *AIP Advances* **5**, 053503 (2015).